

Shape optimisation of singly-symmetric cold-formed steel purlins

V.M. Guimarães^a, B.P. Gilbert^{a,*}, N. Talebian^b, B. Wang^a

^a School of Engineering and Built Environment, Griffith University Gold Coast Campus, Griffith University, QLD, 4222, Australia

^b Faculty of Society & Design, Bond University, Robina QLD 4226, Australia

ARTICLE INFO

Keywords:

Cold-formed steel purlins
Manufacturable purlins
Useable purlins
Shape optimisation

ABSTRACT

This paper presents the results of a study aiming at shape optimising singly-symmetric cold-formed steel purlins. The “self-shape” optimisation algorithm previously developed, proven to be robust and to converge to known solutions is used for this purpose. Eight optimisation cases are considered, consisting of 1.5 mm and 1.9 mm thick purlins, spanning either 3000 mm or 8000 mm and drawn with either 4, 6 or 8 elements per half cross-section. The aim of the algorithm is to minimise the cross-sectional area subjected to the following constraints: (i) the sections must at least match the second moment of area, and the inward and outward bending capacities of commercial purlins used as reference profiles, (ii) be readily manufacturable using existing roll-forming process, (iii) can be connected similarly to existing purlins by offering vertical and horizontal flat elements long enough and strategically positioned to bolt the purlins to gusset plates and screw the roof to them, respectively, and (iv) have an opening wide enough to run services. The restraints provided by the roof sheeting is considered in the algorithm when calculating the bending capacities. Results show that the algorithm converges to consistent solutions and satisfactory satisfies all constraints, resulting in manufacturable and useable purlins. When compared to the reference purlins, the optimised solutions result in saving up to 6.6% of steel. This cost saving in material is quite significant for a mass-produced product such as purlins. The efficiency of the optimised purlins relative to the reference sections were further validated with FE analysis. The FE analyses confirm that the optimised 1.5 mm thick purlins are superior to the reference section. The optimised purlins may therefore benefit the cold-formed steel industry as they represent more economical solutions without compromising on the usability and performance of the products. However, the FE model shows that the 1.9 mm thick purlins may not have the expected performance and experimental testing is fully validate the optimised sections.

1. Introduction

Cold-formed steel (CFS) members are intensively used in civil engineering in various applications such as storage racks, portal frames, wall girts and roof purlins. The latter represents a cost-effective solution to support the roof in many buildings due to its large span to weight ratio [1]. Typically, CFS purlins are thin-walled open cross-sections which are subjected to both inward and outward wind loading (c.f. Fig. 1). The connection between purlins and the roof is typically achieved either through self-tapping screws, interlocking sheeting or standing seam clips [2]. Depending on the type of fasteners used, the roof may add extra rigidity to the purlin members, therefore providing partial lateral, rotational and torsional restraints [2]. These effects should be taken into account to calculate the purlin’s inward and outward bending capacities. The connection to the main frame of the building is generally achieved with the purlins being bolted to gusset plates welded to the

rafters for Cee and Zee purlins [3]. Bridging elements commonly provide lateral and torsional restraint to the purlins.

While efforts have been made to optimise the cross-sectional dimensions of existing purlins in particular or given CFS beams in general [4–10], cross-sectional shape optimisation of CFS purlins has not been performed to date. Cross-sectional shape optimisation consists at finding the optimum cross-sectional shape for given constraints without presumption on the final shape. Several shape optimisation or shape optimisation type algorithms have looked at optimising CFS profiles with [8, 11–14] or without [15–17] practical and manufacturable constraints, yet they usually optimised profiles with no specific end applications in mind. Consequently, this paper aims at shape optimising practical and manufacturable singly-symmetric CFS roof purlins subjected to inward and outward wind loadings. To do so, the paper applies the previous research in Ref. [9,18–21] and intent to inform researchers and industry representatives of optimised and novel purlins which could directly

* Corresponding author.

E-mail address: b.gilbert@griffith.edu.au (B.P. Gilbert).

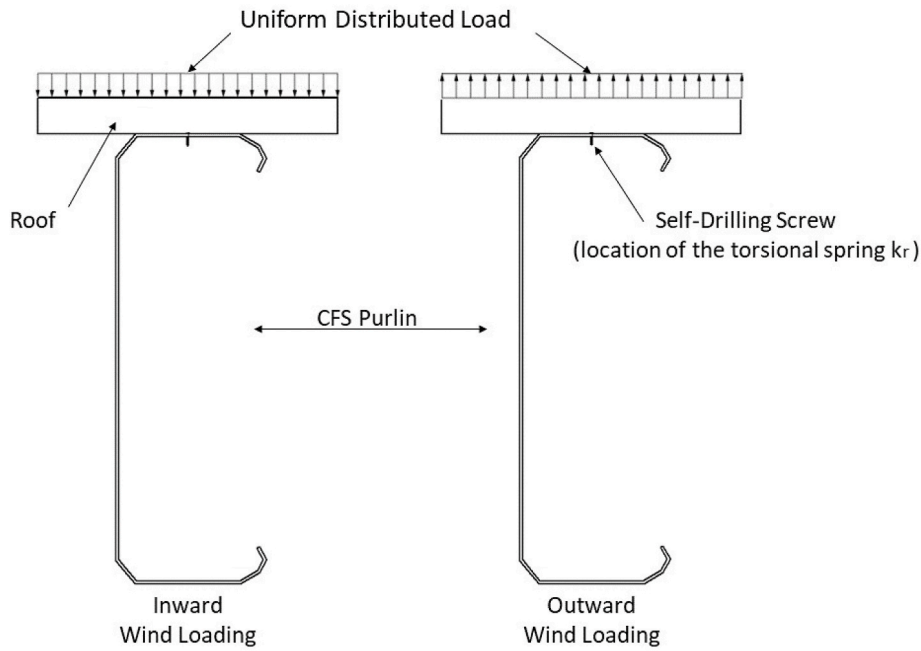


Fig. 1. Purlin attached to roof sheeting and subjected to either inward or outward wind loading.

compete with existing ones. The purlins are optimised to be connected to both the main frame of the building and the roof the same way as currently commercialised Cee purlins [3], therefore ensuring their compatibility to current construction methods. Only the bending and serviceability design criteria are considered in the optimisation process. First, the paper introduces the shape-optimisation algorithm used. Second, the studied optimisation problems are detailed, and the associated design assumptions are explained. Third, the optimised roof purlins are presented. For the sake of computational efficiency, simplified design assumptions were used in the optimisation process. A finite element (FE) model was therefore built and is presented in the last part of the paper to fully validate the efficiency of the optimised purlins relative to existing purlins, used as reference sections. While computationally intensive and not practical for optimisation purpose, FE models allow to more accurately reproduce the loading, restraints and boundary conditions of

cold-formed steel elements and represent a valuable tool to confirm the accuracy of the optimisation algorithm.

2. SHAPE-OPTIMISATION algorithm OF CFS profiles used

2.1. General

The “self-shape” optimisation algorithm developed by Gilbert et al. in Refs. [18,19] and applied in Ref. [9,20,21] to optimise either CFS columns with manufacturing and construction constraints or unconstrained CFS beam-columns is employed in this study. Genetic algorithm (GA) [22,23] is used as the search engine and the Direct Strength Method (DSM) [24], as published in the Australian/New Zealand standard (AS/NZS 4600) [25], is employed to calculate the capacities of the members. Rules have been defined and validated in Refs. [9,18] to

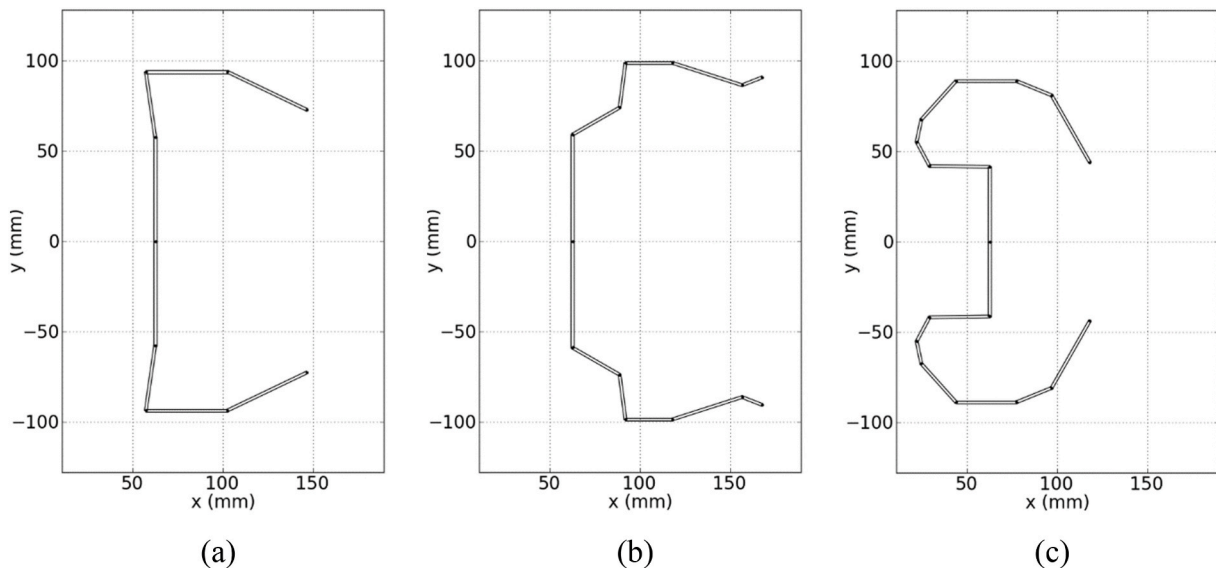


Fig. 2. Examples of cross-sections created in the initial population – (fittest cross-section in the 1st generation shown), with (a) 4 flat elements, (b) 6 flat elements and (c) 8 flat elements per half cross-section.

automatically extract the axial and bending elastic buckling stresses from the signature curves, obtained from the Finite Strip Method (FSM) [26–29]. The accuracy of the algorithm has been validated in Ref. [18, 21] against known optimisation problems for which an analytical solution exists. The augmented Lagrangian constraint handling method (AL) [30] is used in the algorithm to control the penalty parameters and avoid ill-conditioned solutions, therefore ensuring finite values of the penalty factors.

The main operators of the GA-based algorithm to create manufacturable and useable CFS profiles, as published in Ref. [20], are used in this study. Their key principles are summarised in the following subsections. For more details, the reader is kindly referred to Ref. [20].

2.2. Initial population

The initial population is formed by drawing cross-sections from random walks, therefore allowing the creation of cross-sections with no presumptions on their final shape. To create manufacturable CFS profiles, the cross-sections are drawn with a fixed number of flat elements N_e in a given design space (x,y) . This design space is limited in the current research to $x_{\max} = 250$ mm and $y_{\max} = 250$ mm. As singly-symmetric cross-sections are considered in this study, only half of the cross-sections is drawn in the design space. All cross-sections have the same starting point P_0 at the coordinates $(x_{\max}/4, 0)$ [9,18,20].

Usability of the cross-sections are considered by forcing predefined elements to be drawn vertically or horizontally, therefore allowing connections to gusset plates or roof for instance. More details on the location and size of these elements are provided in Sections 3.3.1 and 3.3.2.

The cross-sectional areas in the initial population are evenly distributed to explore more variations in the cross-sectional shapes. A self-avoiding operator is used to prevent the flat elements to cross each other and the design space boundaries, therefore preventing unrealistic cross-sectional shapes to be created.

Fig. 2 shows examples of cross-sections created in the initial population.

2.3. Cross-over

A one-point cross-over operator (CO) performed on the design space is used herein. The two parents selected by the operator must have the same number of flat elements N_e , as well as the same location of horizontal and vertical elements [20]. For the cross-section of $N_e + 1$ cross-sectional points, the cross-over point is randomly chosen between the second and second last points, cutting each parent in two. The first offspring is created following the rules detailed in Ref. [20] from the first and second parts of the first and second parents, respectively, while the second offspring is created from the second and first parts of the first and second parents, respectively. Offsprings therefore share similarities in cross-sectional shape with their parents. The crossover operator produces offsprings with the same number of flat elements N_e as their parents and maintains the elements used for connecting the cross-section to other components horizontal or vertical. Offsprings intersecting themselves are disregarded and new offsprings are then created until the population is replaced.

A CO probability of 0.8 is used in this study. The roulette wheel selection method is employed and only the 50% fittest individuals can enter the mating pool [19]. Elitism is applied and the best two cross-sections per generation are automatically copied to the next generation.

2.4. Mutation

The mutation operator allows the cross-sectional shapes to be altered, therefore creating new shapes, by changing the coordinates of one or more cross-sectional points following the rules in Ref. [20]. Only

the starting point P_0 cannot mutate and is fixed at $(x_{\max}/4, 0)$. The probability of a cross-sectional point to mutate is taken as 0.01.

Similarly to the cross-over operator, this function is programmed so connecting elements stay vertical or horizontal. Mutated cross-sections cannot intersect themselves.

3. Optimisation problem

3.1. General

Eight optimisation scenarios are envisioned in this study. In all cases, the purlins are considered to be simply-supported, singly-symmetric, free to warp and subjected to either a uniformly distributed inward or outward wind load. The purlins are assumed to have a sufficient number of bridges to provide full lateral and torsional restraint, so the bending stress distribution can be obtained from simple bending theory based on the section modulus about an axis perpendicular to the web [2]. More realistic restraints provided by the bridging system is computed in Section 5 when validating the optimised section with FE modelling.

Two spans are considered, (i) a typical span of 8000 mm for which the capacity would principally governed by global buckling, and (ii) a shorter span of 3000 mm for which the capacity can be governed by either local, distortional or global buckling. The yield stress f_y of the purlins is taken as 450 MPa, the Young's modulus E as 200 GPa and the Poisson's ratio ν as 0.3.

Note, while in this paper, the purlins are considered to be singly-symmetric and to be connected to the main frame and roof similarly to commercialised Cee purlins (Section 3.3.2), the algorithm can be applied to optimise other purlin types, such as top hat and point-symmetric purlins, with minor modifications. The location of the restraints provided by the roof (Section 3.3.1) and the opening constraints for services (Section 3.3.3) would have to be changed for the former type, while the symmetric constraints imposed to the algorithm when drawing the cross-sections (Section 2.2) would need to be adapted for point-symmetric purlins.

The roof is assumed to be screwed to the purlins and therefore provides restraints [2], as detailed in Section 3.2.1. The optimisation problem consists at minimising the cross-sectional area subjected to the following constraints: (1) having mechanical properties (inward capacity, outward capacity and bending stiffness) equal to or greater than a commercialised reference purlin enabling it to directly compete with existing products (see Section 3.2), (2) creating a section which could be manufactured (see Section 3.3), (3) enabling connections to the main frame and roof (see Sections 3.3.1 and 3.3.2) and (4) having an opening wide enough to run utilities (see Section 3.3.3). To enable connections to the main frame and roof, segments are set vertical and horizontal, respectively. For each optimisation scenario, the best locations of these segments were found using the methodology detailed in Ref. [20]. As the methodology is already published, the calculations leading to these locations are not presented in this paper.

The optimisations problems considered herein are as follow:

- *Case I:* Shape optimisation of 8000 mm long and 1.5 mm thick purlin manufactured from four flat segments per half cross-section ($N_e = 4$). The first and third segments are set vertical and horizontal, respectively, to connect the purlin. The C20015 purlin (i.e. a lipped Cee-section purlin with a nominal height of 200 mm and a wall thickness of 1.5 mm) commercialised by Lysaght Australia [3] is used as the reference section.
- *Cases II and III:* Same as Case I but with $N_e = 6$ for Case II and $N_e = 8$ for Case III. In both cases, the first segment is kept vertical while the fourth and sixth segments are kept horizontal for Case II and Case III, respectively.
- *Case IV:* Same as Case I but with a wall thickness of 1.9 mm and the C20019 purlin (i.e. a lipped Cee-section purlin with a nominal height

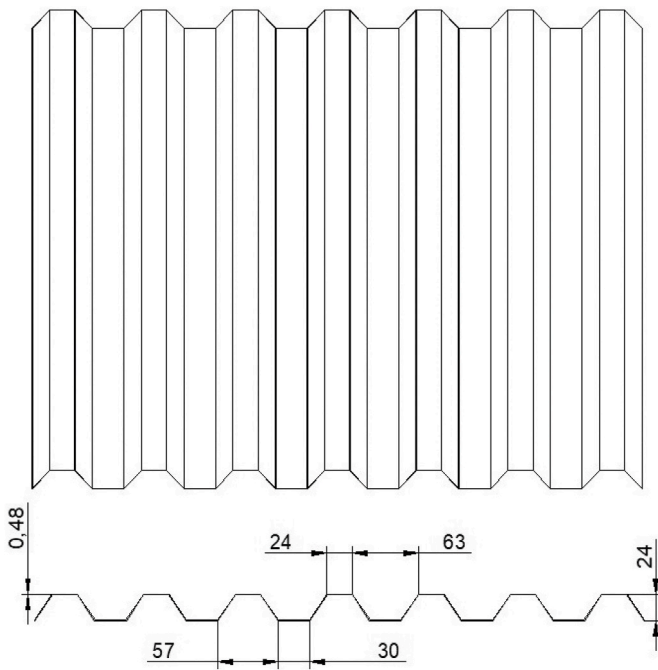


Fig. 3. Dimensions of Lysaght SPANDEK trapezoidal profile [36] considered in this study.

of 200 mm and a wall thickness of 1.9 mm) commercialised by Lysaght Australia [3] used as the reference section.

- Cases V and VI: Same as Case IV but with $N_e = 6$ for Case V and $N_e = 8$ for Case VI. In both cases, the first segment is kept vertical while the

fourth and sixth segments are kept horizontal for Case V and Case VI, respectively.

- Cases VII and VIII: Same as Cases I and IV, i.e. $N_e = 4$, but for 3000 mm long purlins.

Note that in a roll-forming manufacturing process, the cost associated with larger values of N_e is principally linked to the initial set-up of the roll-forming machine. This cost can be offset in mass productions, such as for purlins.

For each optimisation case, the algorithm is run 10 times to verify its robustness. Per run, 400 individuals are created in the initial population and the algorithm is stopped at the 100th generation when convergence has occurred.

3.2. Capacity

3.2.1. Restraints provided by the sheeting

Depending on the type of roof sheeting and the nature of its connection to the purlins, the sheeting can provide either translational restraint, rotational restraint (about an axis perpendicular to the plane of the roof through diaphragm shear action), or torsional restraint [2]. Equations have been developed for these restraints and their influence on the buckling of CFS beams studied [1,31–34]. In developing span tables for Australian purlins, the translational restraint was ignored as it could not be guaranteed that the sheeting would be tied back [35]. This approach is followed in this paper. The diaphragm shear action is also ignored and only the torsional restraint is considered assuming that the roof is screwed to the purlins.

The analytical solution of the torsional restraint k_r for Zeds and Sigmas purlins developed by Zhao et al [34], is adopted in the optimisation process. The solution showed a good agreement between the experimental and theoretical studies, with a 4% difference on average. The equation considers the rotation angle caused by both the localised deformation θ_r of the sheet at the self-drilling screw and the deformation θ_p of the purlin's flange. Two solutions are given in Ref. [34] depending if the purlins rotates so that it contacts the roof at the flange-web intersection or at the flange-lip intersection. The latter equation is conservatively used in this study as it provides the lowest bound value of k_r and is given as:

$$k_r = \frac{E}{\left(\frac{\beta h_T^2}{n t_s^2 a^2} + \frac{a}{3 I_p} + \frac{b}{I_p}\right) L} \quad (1)$$

where $I_p = L t_p^3 / 12 (1 - \nu^2)$, E and ν are the Young's modulus and Poisson's ratio of steel, respectively, L is the purlin's span, t_p and t_s are the purlin and roof sheeting thicknesses, respectively, a and b are the distances from the screws to the left and right ends of the horizontal flange to which the roof is connected, h_T is the purlin flange width, n is the number of screws, β is a coefficient that depends on the b_T/h_T ratio and the screw location in which b_T is the sheet trough width. In this paper, h_T is taken as the width of the horizontal element to which the roof is connected to. The screws are assumed to be positioned in the middle of the horizontal element and a and b are therefore taken as half h_T . β is calculated from Refs. [34] as $0.078 (t_s/0.7)^3$. The roof chosen herein is the 0.48 mm thick Lysaght SPANDEK trapezoidal profile [36] with dimensions given in Fig. 3. The number of screws n considered was extracted from Ref. [36] as function of the purlin's span L and is equal to 15 and 36 for the 3000 mm and 8000 mm long purlins, respectively.

For each cross-section investigated through the optimisation process, the torsional restraint k_r is inputted as a distributed restraint along the length of the profile in the software CUFEM [29] at the location of the screwed connection to calculate the elastic buckling moments, as developed in the next section.

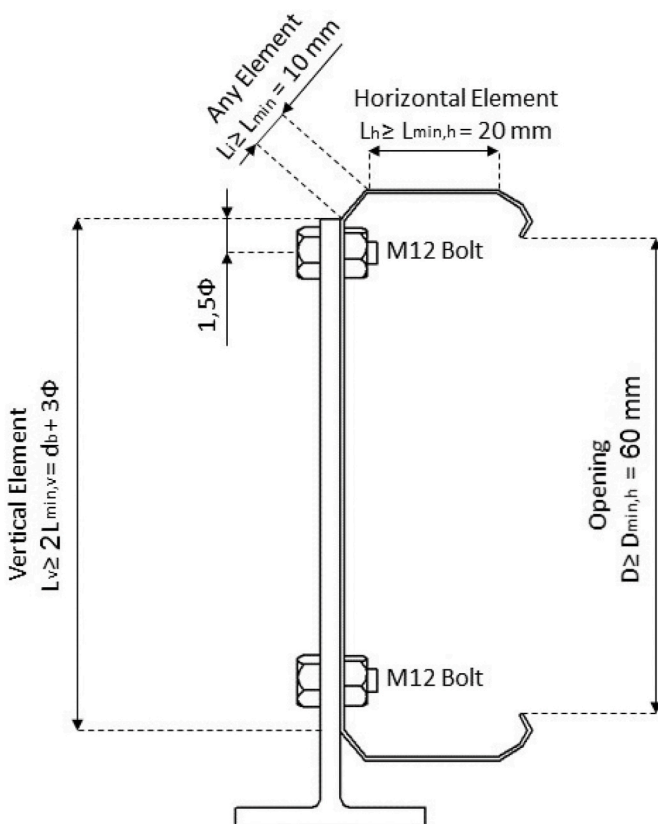


Fig. 4. Manufacturing and assembly constraints.

Table 1
Results for 8000 mm long and 1.5 mm thick purlins – Cases I to III – with reference section.

Case	Section	Properties				Dimensions				
		A_s (mm ²)	I_s (mm ⁴)	M_b^{in} (kN.m)	M_b^{out} (kN.m)	H^c (mm)	W^c (mm)	D^c (mm)	$2 \times L_v^c$ (mm)	L_h^c (mm)
Reference	C20015	579.0	3.80e6	6.02	5.85	203.0	76.0	172.0	203.0	76.0
Case I ($N_e = 4$)	Fittest ^a	550.4	3.80e6	6.04	5.84	218.8	83.6	191.9	170.0	37.1
	2nd fittest ^a	558.7	3.97e6	6.39	6.00	221.9	91.6	212.8	174.6	34.7
	Least fit ^a	574.3	3.87e6	5.95	5.78	208.4	75.5	179.4	197.5	52.3
	Average ^b (CoV)	562.6 (1.56)	3.86e6 (2.39)	6.18 (4.04)	5.96 (3.62)	–	–	–	–	–
Case II ($N_e = 6$)	Fittest ^a	545.5	3.81e6	6.02	5.84	220.0	82.8	203.1	181.5	23.4
	2nd fittest ^a	545.4	3.80e6	6.19	5.85	221.1	87.0	212.4	172.6	28.3
	Least fit ^a	548.0	3.94e6	5.85	5.68	223.9	76.0	197.8	174.3	30.9
	Average ^b (CoV)	553.5 (2.35)	3.83e6 (1.49)	6.33 (8.36)	6.01 (7.29)	–	–	–	–	–
Case III ($N_e = 8$)	Fittest ^a	540.6	3.80e6	6.09	5.84	223.1	84.6	213.1	173.9	20.6
	2nd fittest ^a	554.9	3.79e6	6.39	6.12	216.5	80.7	187.5	168.6	21.0
	Least fit ^a	572.9	3.89e6	6.74	6.16	216.0	100.6	206.9	166.5	21.8
	Average ^b (CoV)	566.7 (2.53)	3.83e6 (1.51)	6.82 (7.80)	6.37 (6.93)	–	–	–	–	–

^a Based on fitness function Eq. (4) with penalty factors of 1.0.

^b Average of 10 runs, coefficient of variation in % given in brackets.

^c Dimension given between cross-sectional nodes, i.e. at centreline of wall elements.

3.2.2. Design rules

As mentioned in Section 2.1, the classical DSM [24], as published in Clause 7.2.2 of the Australian/New Zealand standard AS/NZS 4600 [25], is used by the algorithm to calculate the nominal member moment capacity (M_b) of the purlins. The software CUFSM [29] is used to compute the signature elastic buckling curve from the FSM [26–29]. The rules published and verified in Refs. [9] to automatically obtain the elastic local (M_{ol}) and distortional (M_{od}) buckling moments from the signature curve are used in this study. The elastic global buckling moment (M_o) is directly read from the signature curve at a half-wavelength of either 3000 mm or 8000 mm (i.e. conservatively ignoring the lateral and torsional restraint from the bridging system), and multiplied by a coefficient $C_b = 1.14$ in the AS/NZS 4600 [25] to consider the moment distribution of the simply-supported purlin loaded with a uniformly distributed load (UDL). CUFSM is run twice per investigated cross-section to obtain the elastic buckling moments for both inward and outward wind loadings.

3.3. Manufacturing constraints

In consultation with industry, Wang et al. [21] defined three rules that the final cross-section must satisfy to be deemed manufacturable using roll-forming process. These rules are summarised below:

- **Rule 1:** The minimum length L_{min} of a single flat segment is 10 mm.
- **Rule 2:** The number of segments N_e per half cross-section cannot exceed 10.
- **Rule 3:** For the bend between flat segments, the minimum internal bending radius r to steel sheet thickness t_p ratio is 1.0.

Only Rule 1 is considered in this study and is summarised in Fig. 4. Rule 2 is automatically satisfied in each investigated case (see Section 3.1). As the computational time is strongly correlated to the number of elements entered in CUFSM [29], the roll-forming bending radii are ignored (Rule 3) in the optimisation process and the cross-sections are drawn with sharp angles. Bending radii can be easily added prior to manufacture and was added to the validation of the optimised cross-sections through FE analysis (Section 5). The typical computational time per run using up to 8 cores in a 792-core HPC cluster consisting of a mixture of SGI Altix XE and SGI® Rackable™ C2114-4TY14 servers is 110 h, 140 h and 160 h for half cross-sections drawn with 4, 6 and 8 elements, respectively.

3.3.1. Horizontal elements

The roof is assumed to be screwed to the horizontal element and a minimum length $L_{min,h}$ for this element is considered herein as 20 mm to

allow for that connection. This constraint is illustrated in Fig. 4.

Furthermore, to ensure connection to the roof sheeting, no other element can be positioned above the horizontal element. In the algorithm, the y-axis coordinate of all nodes must be equal to or less than the y-coordinate of the horizontal element.

3.3.2. Vertical elements

Similar size to the currently used gusset plates to connect the purlins, through its vertical element, to the rafters are assumed in this study. Typically, two rows of two holes for M12 bolts are drilled in the gusset plates. The vertical distance d_b between bolts varies with the total depth H of the purlin. Performing a linear regression on current gusset plates in the Lysaght's user guide [3], d_b (in mm) can be approximated to,

$$d_b = 0.9H - 65 \quad (2)$$

Assuming a minimum distance of 1.5φ , where $\varphi = 12$ mm is the bolt's diameter, between the centreline of the holes to the end of the vertical element, the minimum length $L_{min,v}$ of the vertical element of the analysed half cross-section is therefore considered in this study as,

$$L_{min,v} = \frac{d_b}{2} + 1.5\varphi \quad (3)$$

This constraint is illustrated in Fig. 4.

3.3.3. Opening

To allow services to be installed, a minimum opening $D_{min} = 60$ mm of the cross-section is assumed. In the algorithm, the y-axis coordinate of all nodes after the horizontal element must be greater than $D_{min}/2$. This constraint is illustrated in Fig. 4.

3.4. Fitness function and Augmented Lagrangian method

The aim of the optimisation problem is to minimise the cross-sectional area A_s of the purlin subjected to the previously listed constraints. The unconstrained fitness function f suitable for GA is expressed in terms of inequality constraints as,

$$f = \frac{A_s}{A_{ref}} + \alpha_{in} \max\left(0, \frac{M_b^{in}}{M_b^{in}} - 1\right) + \alpha_{out} \max\left(0, \frac{M_b^{out}}{M_b^{out}} - 1\right) + \alpha_I \max\left(0, \frac{I_{ref}}{I_s} - 1\right) + \sum_{i=1}^{N_e} \alpha_{L,i} \max\left(0, \frac{L_{min,i}}{L_{s,i}} - 1\right) + \sum_{j=h}^{N_e+1} \alpha_{D,j} \max\left(0, \frac{D_{min}}{2y_j} - 1\right) + \alpha_h \max\left(0, \frac{y_{max}}{y_h} - 1\right) \quad (4)$$

where A_{ref} is the cross-sectional area of the reference purlin, M_b^{in} and M_b^{out} are the inward and outward bending capacities, respectively, of

the purlin, $M_{b,ref}^{in}$ and $M_{b,ref}^{out}$ are the inward and outward bending capacities, respectively, of the reference purlin, I_s and I_{ref} are the second moments of area of the purlin and reference purlin, respectively, $L_{min,i}$ and $L_{s,i}$ are the minimum required length and actual length, respectively, of segment number i , h is the index number of the last node of the horizontal element, y_j is the y-coordinates of node number j and y_{max} is the maximum y-coordinate of all nodes. α_{ins} , α_{outs} , α_I , $\alpha_{L,i}$, $\alpha_{D,j}$, and α_h are penalty factors. In Eq. (4), (i) the first term represents the objective, (ii) the second and third terms correspond to the constraints on the inward and outward bending capacities relative to the reference section, (iii) the fourth term defines the constraint on the bending stiffness, also related to the reference section, (iv) the fifth term specifies the constraint on the minimum length on all elements (Sections 3.3, 3.3.1 and 3.3.2), (v) the sixth term stipulates the minimum opening of the cross-section (Section 3.3.3) and (vi) the last term sets the location of the horizontal segment at the extreme fibre of the cross-section (Section 3.3.1).

As stipulated in Section 3.1, the Augmented Lagrangian method [30] is used in the algorithm to express the fitness function and avoid ill-conditioned problems. AL has been successfully used in shape-optimisation of CFS beams and columns in Refs. [9,20,21]. More information on AL can be found in Ref. [30,37] and its specific application to the current problem in Refs. [19]. The AL fitness function f_{AL} is expressed as,

$$f_{AL} = \frac{A_s}{A_{ref}} + \frac{1}{2} \left\{ \gamma_{in} \left[\max \left(0, \frac{M_{b,ref}^{in}}{M_b^{in}} - 1 + \mu_{in} \right) \right]^2 + \gamma_{out} \left[\max \left(0, \frac{M_{b,ref}^{out}}{M_b^{out}} - 1 + \mu_{out} \right) \right]^2 + \gamma_I \left[\max \left(0, \frac{I_{ref}}{I_s} - 1 + \mu_I \right) \right]^2 + \sum_{i=1}^{N_e} \gamma_{L,i} \left[\max \left(0, \frac{L_{min,i}}{L_{s,i}} - 1 + \mu_{L,i} \right) \right]^2 + \sum_{j=h}^{N_e+1} \gamma_{D,j} \left[\max \left(0, \frac{D_{min}}{2y_j} - 1 + \mu_{D,j} \right) \right]^2 + \gamma_h \left[\max \left(0, \frac{y_{max}}{y_h} - 1 + \mu_h \right) \right]^2 \right\} \tag{5}$$

where γ_{ins} , γ_{outs} , γ_I , $\gamma_{L,i}$, $\gamma_{D,i}$ and γ_h are the penalty function coefficients, and μ_{ins} , μ_{outs} , μ_I , $\mu_{L,i}$, $\mu_{D,i}$ and μ_h are the real parameters associated with the penalty function coefficients. The initial values of these parameters are chosen herein based convergence studies performed in Ref. [9,18,20] as 2.0 for the penalty function coefficients and zero for the real parameters. The AL convergence rate is taken as 1.5 and the penalty increasing constant as 1.05 [18,19].

For consistency and sake of comparison, the inward $M_{b,ref}^{in}$ and outward $M_{b,ref}^{out}$ bending capacities, the cross-sectional area A_{ref} and the

second moment of area I_{ref} of the reference purlins are calculated using the same rules as the optimised sections and with sharp corners. The properties of these sections are given in Table 1 and Table 2 for 8000 mm long purlins and in Table 3 and Table 4 for 3000 mm long purlins.

4. Results and discussion

4.1. Convergence

Fig. 5 plots the average fitness over 10 runs, calculated from Eq. (4) with penalty factors equal to 1.0, for all analysed cases in Section 3.1. Convergence is always achieved, generally before reaching 60 generations, outlining the robustness of the algorithm. The higher the number of flat elements, the slower the convergence rate as the algorithm needs to explore a larger design space.

4.2. Constraints

The algorithm always adequately satisfies all constraints and therefore produces solutions which can directly compete with existing products, be manufactured and assembled:

- **Constraints on properties:** the algorithm satisfies the constraints on the

inward capacity, the outward capacity and the second moment of area for 88.8%, 66.2% and 60% of the runs performed, respectively. When these constraints are not satisfied, the error is small and is on average equal to 1.0% for M_b^{in} , 1.1% for M_b^{out} and 0.87% for I_s .

- **Constraints on manufacturing:** all elements of a cross-section fulfil the minimum length requirements for more than 61% of the runs. When this constraint is not satisfied, the average accumulated error over all elements is small and equal to 0.5%. This error is typically larger for $N_e = 8$ than for $N_e = 4$.

Table 2
Results for 8000 mm long and 1.9 mm thick purlins – Cases IV to VI – with reference section.

Case	Section	Properties				Dimensions				
		A_s (mm ²)	I_s (mm ⁴)	M_b^{in} (kN.m)	M_b^{out} (kN.m)	H^c (mm)	W^c (mm)	D^c (mm)	$2 \times L_v^c$ (mm)	L_h^c (mm)
Reference	C20019	746.7	4.91e6	8.77	8.57	203.0	76.0	165.0	203.0	76.0
Case IV ($N_e = 4$)	Fittest ^a	711.8	5.05e6	8.78	8.53	221.5	86.8	196.3	180.4	38.3
	2nd fittest ^a	711.9	4.89e6	9.06	8.75	213.2	90.8	194.2	164.9	56.8
	Least fit ^a	738.0	5.17e6	10.51	9.98	217.4	100.9	196.2	165.4	40.0
	Average ^b (CoV)	722.6 (1.55)	5.00e6 (3.10)	9.35 (7.45)	8.99 (6.52)	–	–	–	–	–
Case V ($N_e = 6$)	Fittest ^a	710.0	4.92e6	8.87	8.58	218.5	80.7	192.3	175.2	33.5
	2nd fittest ^a	709.7	4.91e6	9.51	9.15	217.5	92.6	199.2	169.0	28.7
	Least fit ^a	740.5	4.92e6	9.18	8.60	207.8	108.1	203.3	160.5	29.6
	Average ^b (CoV)	719.4 (1.87)	4.92e6 (0.16)	9.17 (3.37)	8.79 (3.42)	–	–	–	–	–
Case VI ($N_e = 8$)	Fittest ^a	706.1	4.91e6	8.98	8.59	217.6	89.7	205.2	169.1	21.9
	2nd fittest ^a	713.3	4.91e6	9.60	9.10	217.3	96.0	210.0	169.0	26.5
	Least fit ^a	777.0	4.90e6	10.31	9.42	197.4	123.2	190.1	150.6	24.8
	Average ^b (CoV)	747.1 (3.48)	4.91e6 (0.17)	10.19 (12.5)	9.47 (12.1)	–	–	–	–	–

^a Based on fitness function Eq. (4) with penalty factors of 1.0.

^b Average of 10 runs, coefficient of variation in % given in brackets.

^c Dimension given between cross-sectional nodes, i.e. at centreline of wall elements.

Table 3
Results for 3000 mm long and 1.5 mm thick purlins – Case VII – with reference section.

Case	Section	Properties				Dimensions				
		A_s (mm ²)	I_s (mm ⁴)	M_b^{in} (kN.m)	M_b^{out} (kN.m)	H^c (mm)	W^c (mm)	D^c (mm)	$2 \times L_v^c$ (mm)	L_h^c (mm)
Reference	C20015	579.0	3.80e6	9.41	9.03	203.0	76.0	172.	203.	76.
Case VII ($N_e = 4$)	Fittest ^a	547.0	3.82e6	9.93	9.03	220.0	75.5	193.9	179.0	46.1
	2nd fittest ^a	553.5	3.83e6	9.78	9.37	217.7	80.8	190.6	191.4	39.3
	Least fit ^a	598.3	3.98e6	10.25	9.81	204.4	87.4	170.1	204.4	48.6
	Average ^b (CoV)	565.6 (2.84)	3.85e6 (2.15)	10.03 (4.32)	9.42 (5.46)	–	–	–	–	–

^a Based on fitness function Eq. (4) with penalty factors of 1.0.
^b Average of 10 runs, coefficient of variation in % given in brackets.
^c Dimension given between cross-sectional nodes, i.e. at centreline of wall elements.

Table 4
Results for 3000 mm long and 1.9 mm thick purlins – Cases VIII – with reference section.

Case	Section	Properties				Dimensions				
		A_s (mm ²)	I_s (mm ⁴)	M_b^{in} (kN.m)	M_b^{out} (kN.m)	H^c (mm)	W^c (mm)	D^c (mm)	$2 \times L_v^c$ (mm)	L_h^c (mm)
Reference	C20019	746.7	4.91e6	14.66	14.24	203.0	76.0	165.0	203.0	76.0
Case VIII ($N_e = 4$)	Fittest ^a	720.4	4.87e6	14.98	14.25	215.1	86.3	178.6	186.0	34.2
	2nd fittest ^a	729.6	5.19e6	15.32	14.70	218.6	86.1	186.5	193.4	45.5
	Least fit ^a	729.1	4.63e6	15.05	13.90	204.9	98.7	176.9	169.8	38.8
	Average ^b (CoV)	730.2 (0.87)	4.921e6 (3.58)	15.37 (3.26)	14.58 (2.82)	–	–	–	–	–

^a Based on fitness function Eq. (4) with penalty factors of 1.0.
^b Average of 10 runs, coefficient of variation in % given in brackets.
^c Dimension given between cross-sectional nodes, i.e. at centreline of wall elements.

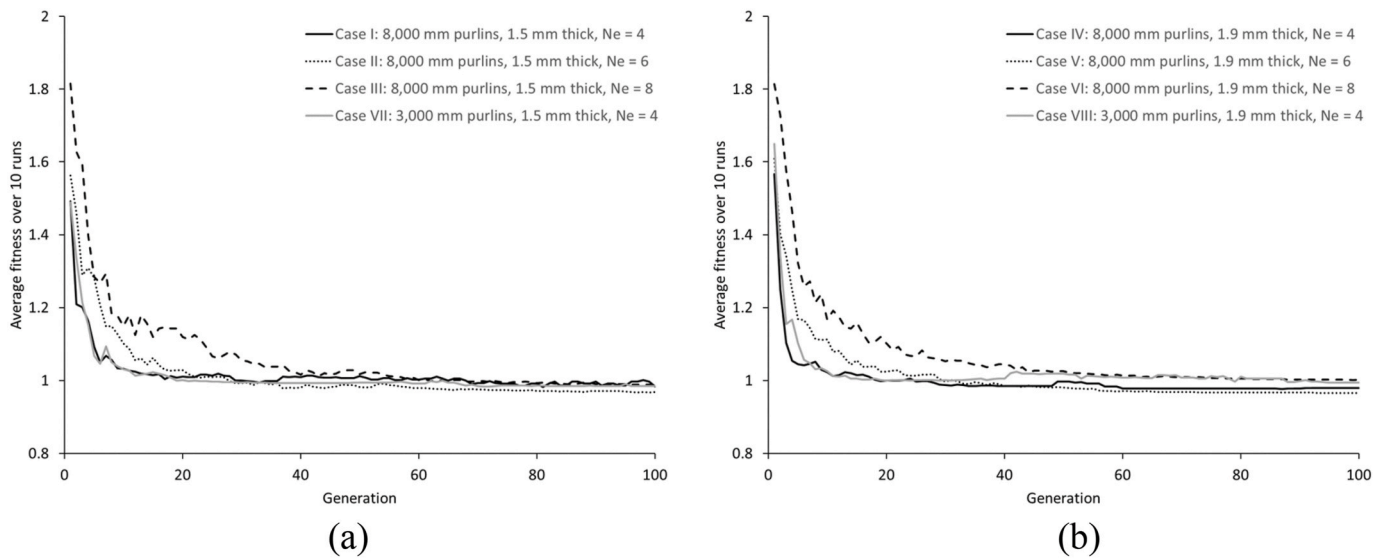


Fig. 5. Average fitness over 10 runs for (a) 1.5 mm thick purlins and (b) 1.9 mm thick purlins.

- **Constraints on assembly:** (i) the constraint on the minimum opening is always satisfied and (ii) the horizontal flat segment is located at the extreme fibre of the cross-section for 88.8% of the runs, with also a small average error of 0.4% when this constraint is not satisfied.

4.3. Optimised purlins

4.3.1. Cases I to III – 8000 mm long and 1.5 mm thick purlins

Table 1 summarises the properties and dimensions of the fittest, 2nd fittest and least fit cross-sections over 10 runs for Cases I to III. Eq. (4), with penalty factors equal to 1.0, is used to determine the fitness of a cross-section. The average properties over 10 runs, with associated coefficients of variation (CoV), are also provided in the table for information and to outline the consistency of the solutions. The cross-sections reported in Table 1 are also plotted in Fig. 6, Fig. 7 and Fig. 8 for Case I, Case II and Case III, respectively.

Results show that increasing the number of flat segments leads to a reduction of the optimised cross-sectional area. Similarly to Ref. [9,18], the larger the number of elements, the more the algorithm smooths and rounds the cross-sections. When compared to the reference section C20015, the optimised (fittest) cross-sections drawn with 4, 6 and 8 flat elements per half cross-section result in saving 4.9%, 5.7% and 6.6% of steel, respectively. This cost saving in material is quite significant for a mass-produced product such as purlins. Therefore, the optimised purlins presented in the paper may benefit the industry as they are readily manufacturable with existing roll-forming process, can be connected to the rafters and roof using the fasteners currently used and they have properties matching existing purlins. Note that the optimised purlins are however between 6% and 10% deeper than the reference section and up to 31% wider.

In reference to Figs. 7 and 8, the algorithm tends to nearly align some of the flat segments between the vertical and horizontal elements, and

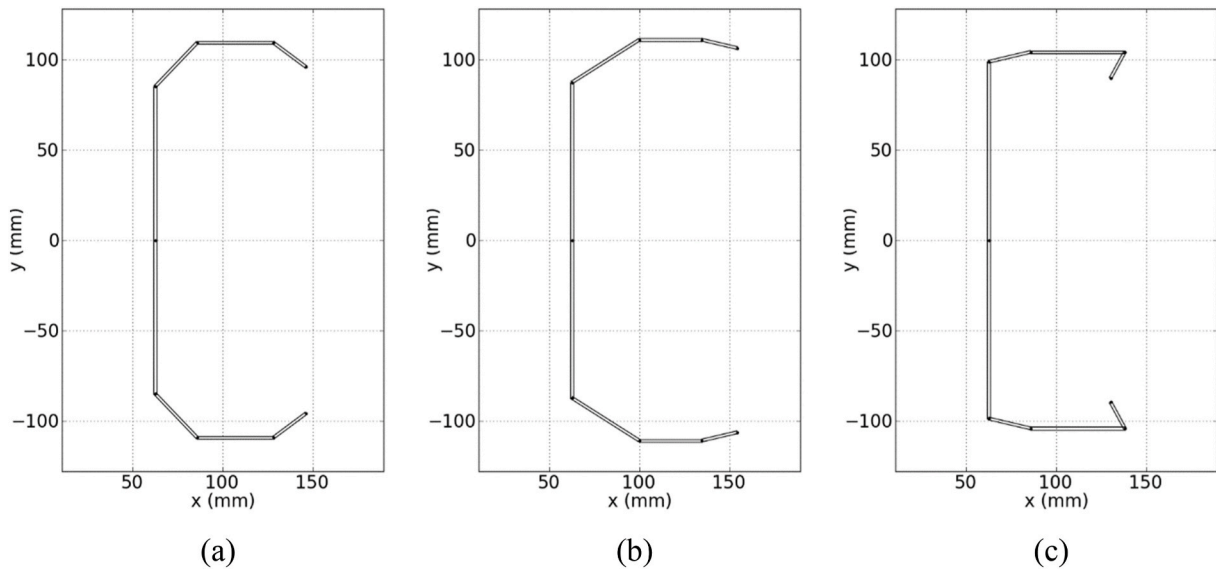


Fig. 6. Case I (8000 mm long, 1.5 mm thick and $N_e = 4$) results (a) fittest cross-section, (b) 2nd fittest cross-section and (c) least fit cross-section.

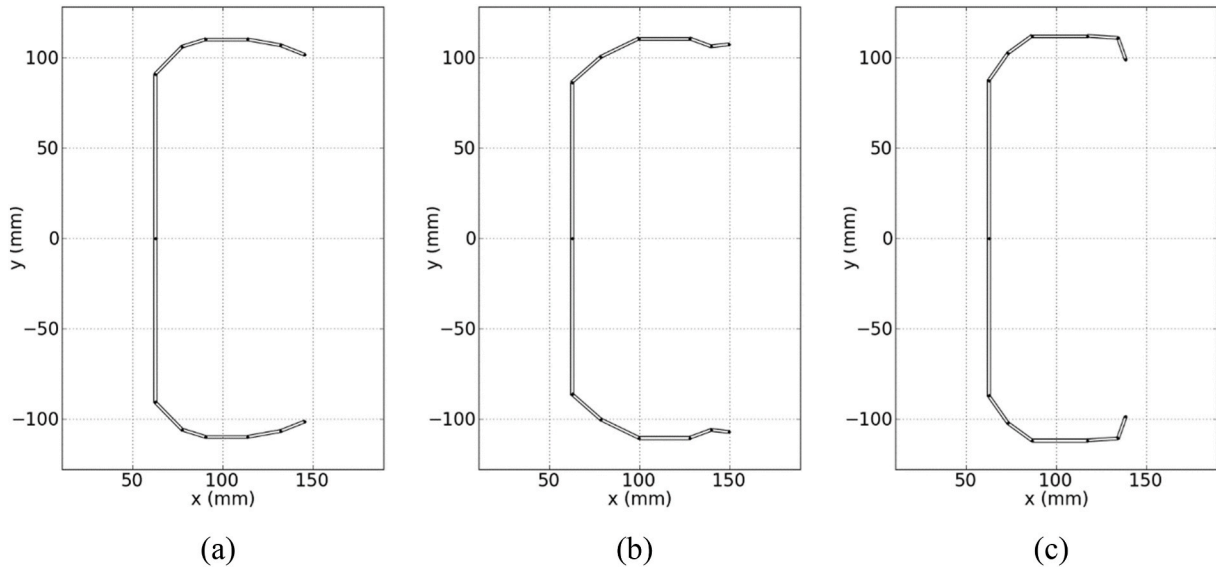


Fig. 7. Case II (8000 mm long, 1.5 mm thick and $N_e = 6$) results (a) fittest cross-section, (b) 2nd fittest cross-section and (c) least fit cross-section.

for practicality, a manufacturer may choose to reduce the number of cross-sectional elements by merging these nearly aligned flat segments, therefore favouring the optimised cross-sections in Case I.

4.3.2. Cases IV to VI – 8000 mm long and 1.9 mm thick purlins

Table 2 summarises the same results as Table 1, but for Cases IV to VI. The cross-sections reported in Table 2 are plotted in Fig. 9, Fig. 10 and Fig. 11 for Case IV, Case V and Case VI, respectively. Similar conclusions to Section 4.3.1 can be drawn: (i) when compared to the reference section C20019, the optimised cross-sections drawn with 4, 6 and 8 flat elements per half cross-section result in saving 4.7%, 4.9% and 5.4% of steel, respectively, and (ii) the optimised cross-sections are typically deeper and wider than the reference section. The presented solutions therefore also represent more economical purlins.

Similar to Cases II and III, in Cases V and VI, some flat segments are nearly aligned between the vertical and horizontal elements, and a manufacturer may choose to merge these segments for practicality.

4.3.3. Cases VII and VIII – 3000 mm long purlins

Tables 3 and 4 summarise the same results as Table 1, but for Cases VII and VIII, respectively. Figs. 11 and 12 plot the cross-sections reported in Tables 3 and 4, respectively. The optimised cross-sectional shapes for the 3000 mm long purlins are very similar to the ones found for the 8000 mm long purlins. Similar savings in steel than for Cases I and IV can be achieved for Case VII (5.5% savings) and Case VIII (3.5% savings) (see Fig. 13).

For the 1.5 mm thick optimised purlins, the local, distortional and global buckling modes govern the inwards and outwards capacities for 55%, 25% and 20% of the cases, respectively. However, for the 1.9 mm thick optimised purlins, the same buckling modes govern for 10%, 30% and 60% of the cases, respectively. Still for the 1.9 mm thick optimised purlins, when global buckling governs, the distortional capacity is on average only 4% higher than the global capacity. Buckling mode interaction may therefore take place as noted in Ref. [18].

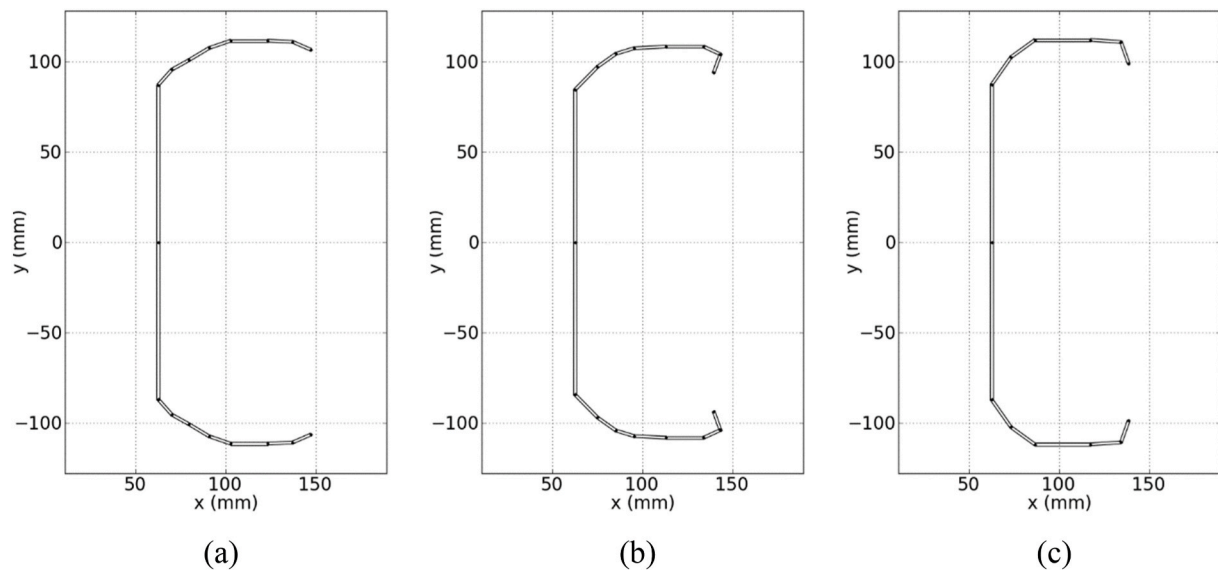


Fig. 8. Case III (8000 mm long, 1.5 mm thick and $N_e = 8$) results (a) fittest cross-section, (b) 2nd fittest cross-section and (c) least fit cross-section.

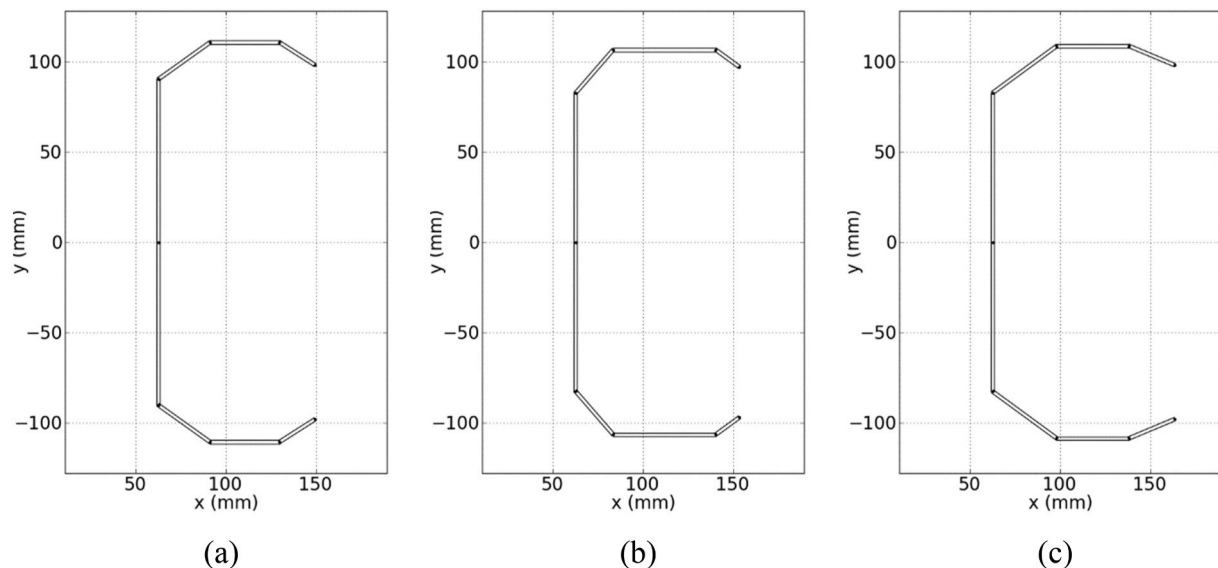


Fig. 9. Case IV (8000 mm long, 1.9 mm thick and $N_e = 4$) results (a) fittest cross-section, (b) 2nd fittest cross-section and (c) least fit cross-section.

5. Finite element analysis

The efficiency of the optimised purlins relative to the reference sections are now validated with FE analysis. FE analysis is a well mature numerical method to model the structural response of cold-formed steel elements (see Refs. [38–40] for instance), with guidance provided in Ref. [41]. However, as computationally intensive, it is not always well suited for optimisation problems for which simplified design assumptions must often be made, as in the present paper (see Section 3). Nevertheless, by more accurately reproducing the loading, restraints and boundary conditions it represents a valuable tool to verify and confirm the optimisation results.

In the section, the fittest cross-sections for Cases I and IV, and the C20015 and C20019 reference sections are modelled using the FE software Abaqus [42]. The bending stiffness, inward and outward capacities of these sections are compared.

5.1. Finite element model

5.1.1. General

The FE model is represented in Fig. 14. The bending radius was added to all cross-sections, with the internal bending radius r taken as 1.0 times the wall thickness t . A positive or negative uniformly distributed pressure was applied to the top flange of the purlin, as shown in Fig. 14, to simulate the inward and outward wind loads, respectively. S4R shell elements were used with a mesh size of $3 \text{ mm} \times 3 \text{ mm}$, arising from the mesh sensitivity analyses in Ref. [38]. Non-linear geometric and material Riks analyses were run.

5.1.2. Material properties

In the flat parts of the cross-sections, the yield f_y and ultimate f_u stresses were taken as 450 MPa (Section 3.1) and 520 MPa [25], respectively. The strain-stress curve considered in these parts is shown in Fig. 15 and extracted from the coupon tests performed on cold-formed steel samples of similar yield stress in Ref. [38].

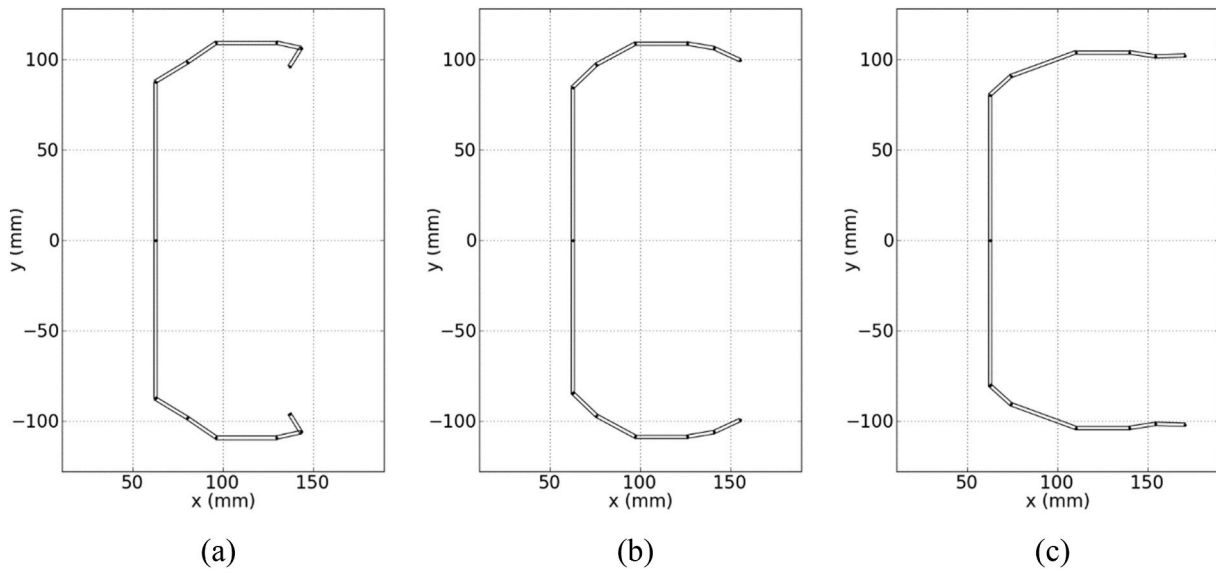


Fig. 10. Case V (8000 mm long, 1.9 mm thick and $N_e = 6$) results (a) fittest cross-section, (b) 2nd fittest cross-section and (c) least fit cross-section.

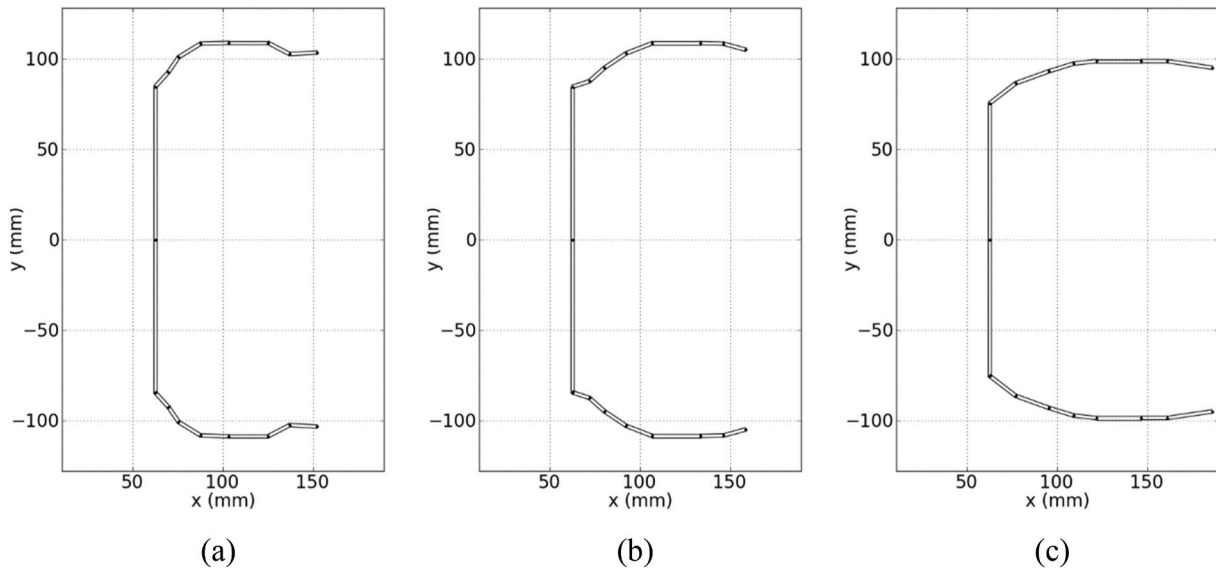


Fig. 11. Case VI (8000 mm long, 1.9 mm thick and $N_e = 8$) results (a) fittest cross-section, (b) 2nd fittest cross-section and (c) least fit cross-section.

To account for the cold-forming process, the yield stress f_y was enhanced by Δf_y in the corners, and over a distance equal to $0.5\pi r$ on each side of a corner (Fig. 14), following the equations in Ref. [43]:

$$\Delta f_y = 0.6 \left(\frac{B_c}{(r/t)^m} - 1 \right) f_y \quad (6)$$

where,

$$m = 0.192 \left(\frac{f_u}{f_y} \right) - 0.068 \quad (7)$$

$$B_c = 3.69 \left(\frac{f_u}{f_y} \right) - 0.819 \left(\frac{f_u}{f_y} \right)^2 - 1.79 \quad (8)$$

An elastic-perfectly plastic strain-stress curve was considered in the corners. For both flat parts and corner, true stress-strain curves were inputted into the software [44].

5.1.3. Boundary conditions and restraints

Similar to the optimisation process, the purlins were considered to be simply supported. To simulate the connections to the rafters, at each end of the purlin, the nodes of the web over a 36 mm wide ($3 \times$ bolt diameter) \times twice $L_{\min,v}$ high (gusset plate height in Eq. (3)) area were constrained as shown in Fig. 14.

Three rows of bridging were considered, with the first and last rows positioned at 0.28 times the purlin span [3]. At each row of bridging, the lateral displacement of the nodes of the web over a 36 mm wide \times 150 mm high area were restrained, as shown in Fig. 14.

The torsional restraints k_r provided by the roof and considered in the optimisation algorithm (Eq. (1)), was simulated at the location of the 36 screws for the 8000 mm long purlin, as shown in Fig. 14.

5.1.4. Imperfections

The strength and post-buckling behaviour of cold-formed steel members are sensitive to geometric imperfections. Imperfections were considered in this study by scaling the first buckling mode, obtained from a linear buckling analysis, so that the maximum imperfection was

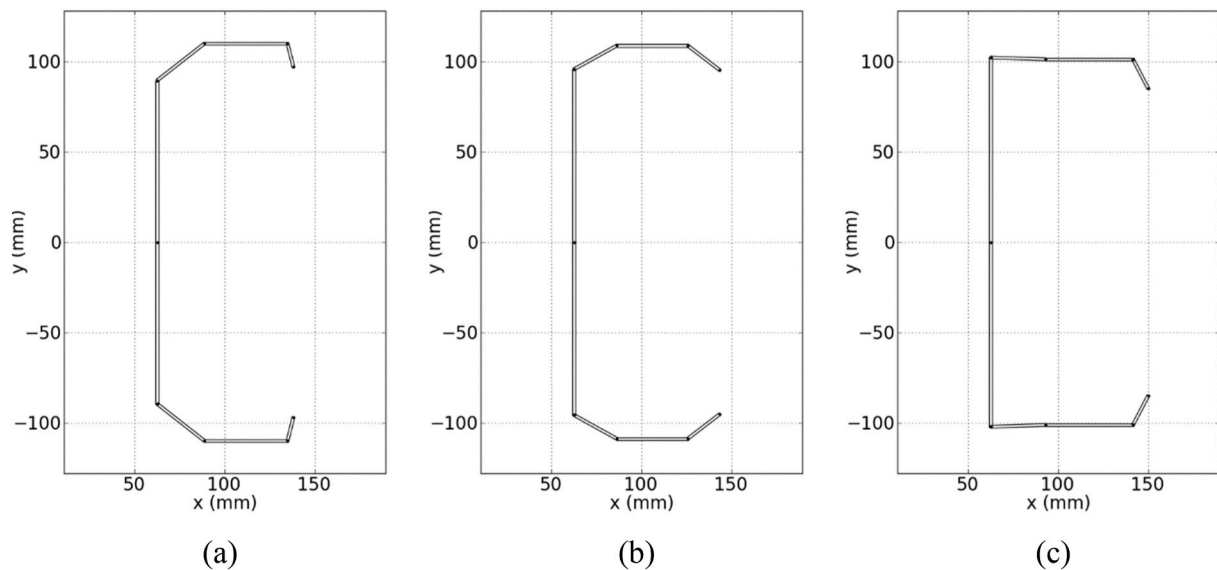


Fig. 12. Case VII (3000 mm long, 1.5 mm thick and $N_e = 4$) results (a) fittest cross-section, (b) 2nd fittest cross-section and (c) least fit cross-section.

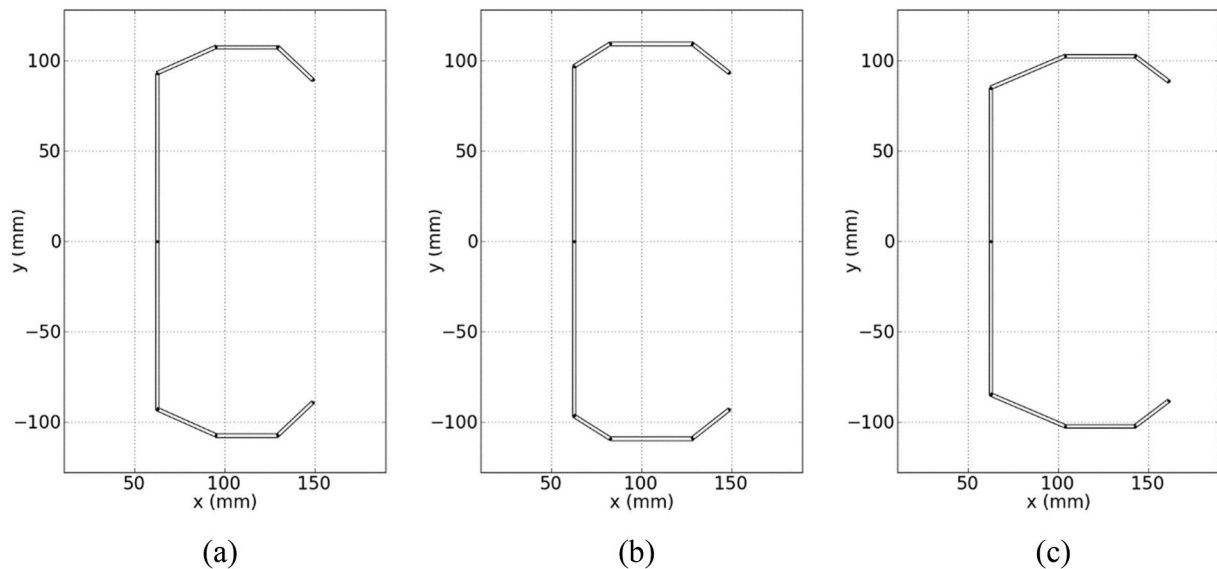


Fig. 13. Case VIII (3000 mm long, 1.9 mm thick and $N_e = 4$) results (a) fittest cross-section, (b) 2nd fittest cross-section and (c) least fit cross-section.

either equal to the span/1000, if the first buckling mode was global, or $0.1t$, otherwise [41].

5.2. Finite element results

Table 5 summarises the cross-sectional area, the bending stiffness (in kN/mm) and the maximum inward and outward applied loads (in kN) of the analysed cross-sections. In the table, the bending stiffnesses were calculated by performing a linear regression on the applied load versus deflection at mid-span and middle of the web relationships. Note that the cross-sectional areas in Table 5 differ from Tables 1 and 2 due to the bending radius being considered in the FE models and not in the optimisation algorithm.

The inward and outward failure modes for C20015 and Case I are plotted in Fig. 16. Failure occurred by local buckling of the flange in compression.

For all scenarios, the bending stiffness of the optimised purlin is

always higher than or equal to the associated reference purlin. For the 1.5 mm thick purlins, the capacity of the optimised purlin is between 11% (outward) and 16.9% (inward) greater than the reference C20015 purlin. This leads to the capacity to cross-sectional area ratio of the optimised purlin being between 15.7% and 21.9% greater than the reference purlin. This confirms and outperforms the prediction of the optimisation algorithm. For the 1.9 mm thick purlins, the inward capacities of the optimised and reference purlins are equal, confirming the prediction of the algorithm. However, the outward capacity of the reference purlin is 5% greater than the optimised purlin. In term of capacity to cross-section area ratios, for inward loading the optimised purlin outperforms the C20019 by 3.9%, however, the reference purlin outperforms the optimised section by 1.6% for outward loading.

While the FE models confirm the potential of the 1.5 mm thick optimised purlins, the optimised 1.9 mm thick purlins may not have the expected performance. Experimental tested are still needed to confirm these results.

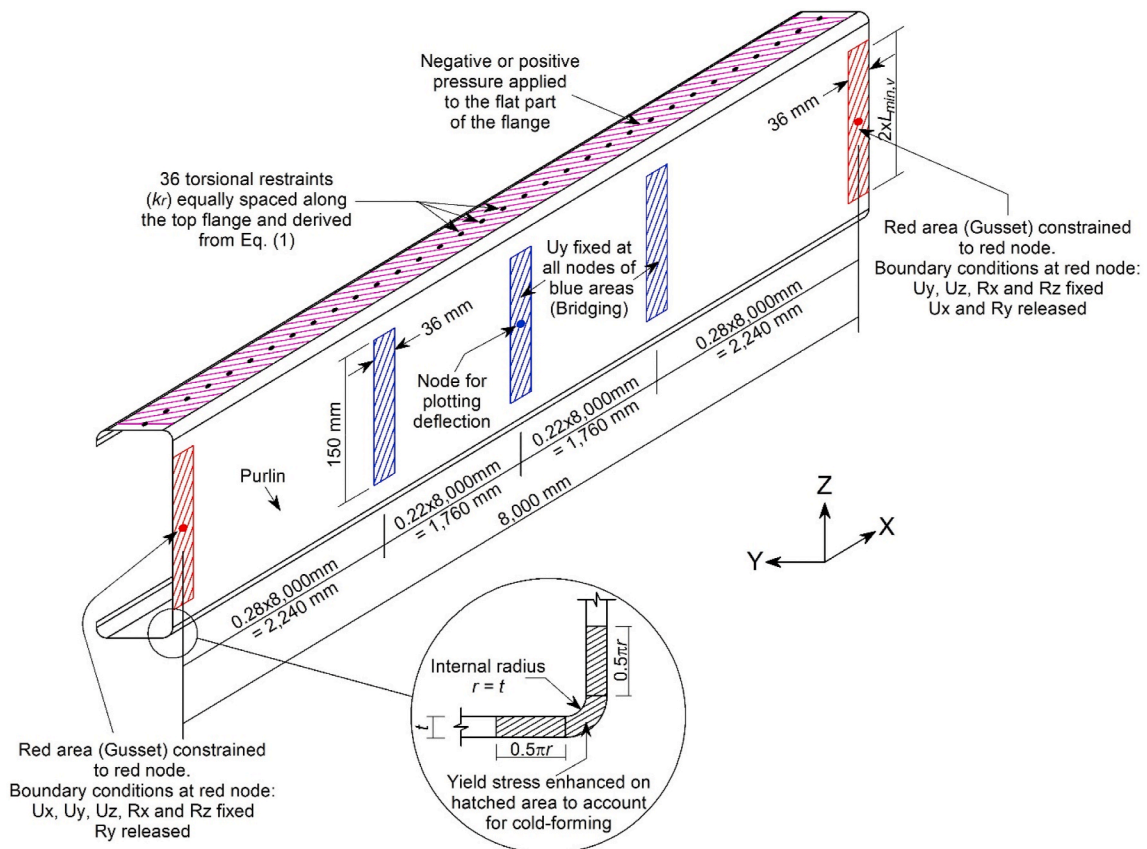


Fig. 14. Overview of the FE model.

6. Conclusions

This paper shape optimised manufacturable and useable singly-symmetric purlins which can directly compete with existing products. The algorithm was presented along with the design methodology and the constraints considered. Eight optimisation cases were considered by optimising 1.5 mm and 1.9 mm thick purlins spanning either 3000 mm or 8000 mm. The cross-sections were drawn with either 4, 6 or 8 elements per half cross-section. Results showed that the algorithm converged to consistent solutions and satisfactory satisfied all constraints, resulting in optimised purlins which (i) can be manufactured with existing roll-forming process, (ii) be connected to the rafters and roof using the fasteners currently used and (iii) have properties matching commercial purlins used as references. When compared to these reference purlins, the optimised purlins would save up to 6.6% of steel and therefore represent a potential solution to produce more economical products without compromising on their performance. The efficiency of the optimised purlins relative to the reference sections were further validated with FE analysis. The FE model more accurately reproduced the loading, restraints and boundary conditions when compared to the design assumptions made in the optimisation process. The FE analyses confirm that the optimised 1.5 mm purlins are superior to the reference

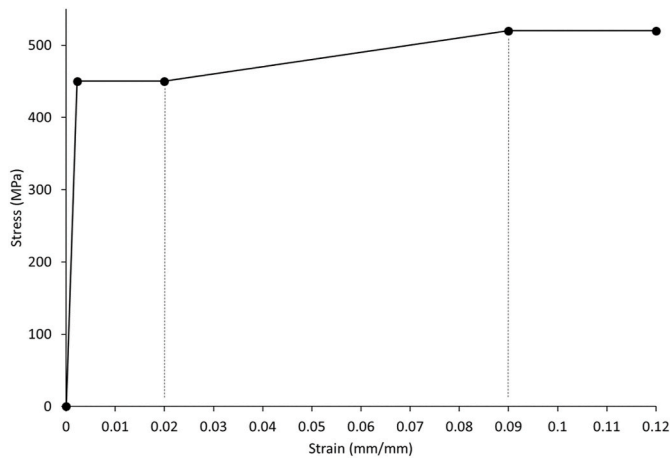


Fig. 15. Stress-strain curve used for flat part of the cross-section.

Table 5
Finite element results.

Case/section	A_s (mm ²)	Inward			Outward		
		Stiffness (kN/mm)	Capacity (kN)	Capacity to area ratio (N/mm)	Stiffness (kN/mm)	Capacity (kN)	Capacity to area ratio (N/mm)
C20015	573.2	0.108	10.4	18.2	0.111	10.2	17.8
Case I	549.7	0.109	12.2	22.2	0.113	11.3	20.6
C20019	737.4	0.141	17.9	24.2	0.143	17.1	23.2
Case IV	710.2	0.147	17.9	25.2	0.150	16.2	22.8

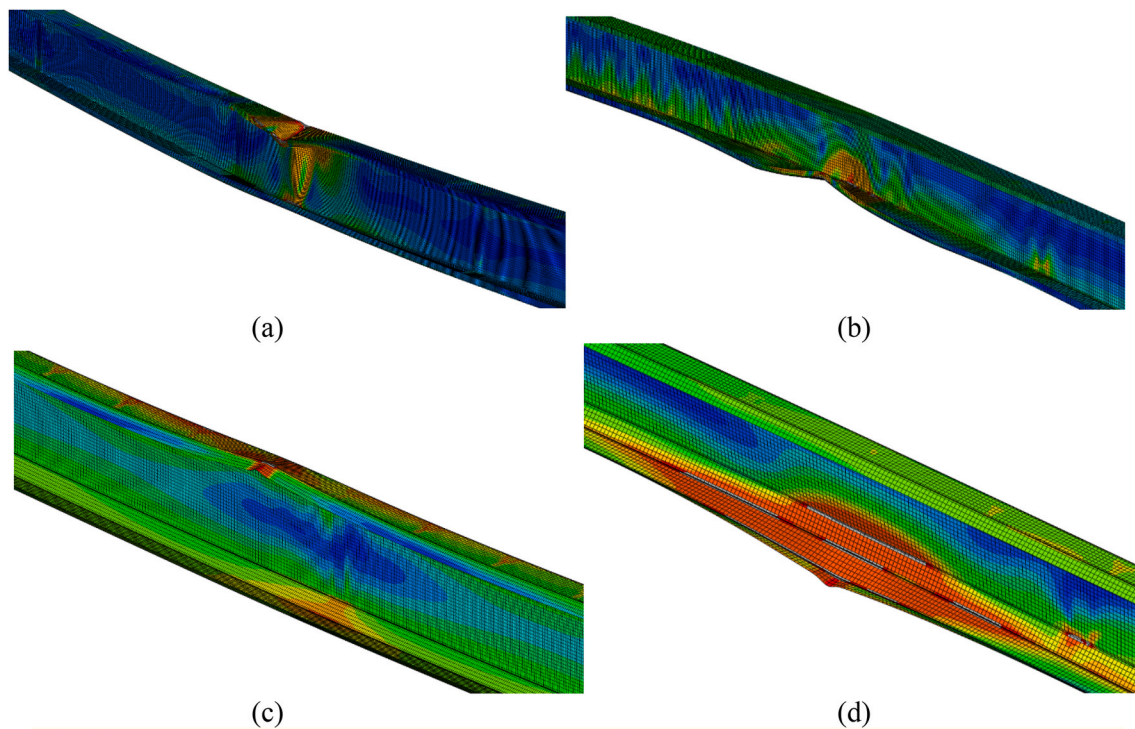


Fig. 16. FE failure for (a) inward loading for C20015, (b) outward loading for C20015, (c) inward loading for Case I and (d) outward loading for Case I.

section, however, the 1.9 mm thick purlins may not have the expected performance. The next step to this research would be to experimentally verify the new and optimised purlins to fully investigate their potential and consider possible buckling mode interactions.

Credit author statement

V.M. Guimarães: Conceptualization, Methodology, Software, Investigation, Writing – original draft. B.P. Gilbert: Conceptualization, Methodology, Visualization, Writing – original draft, Supervision. N. Talebian: Software, Validation. B. Wang: Conceptualization, Methodology, Software.

Declaration of competing interest

The authors declare that they have no known competing financial interests or personal relationships that could have appeared to influence the work reported in this paper.

Acknowledgements

Emeritus Professor Gregory Hancock from the University of Sydney, Australia, is thanked for the discussions and advices on purlin design.

References

- [1] Z.-M. Ye, R. Kettle, L.-Y. Li, Analysis of cold-formed zed-purlins partially restrained by steel sheeting, *Comput. Struct.* 82 (2004) 731–739.
- [2] G.J. Hancock, *Design of Cold-Formed Steel Structures* (To AS/NZ 4600:2007), fourth ed., Australian Steel Institute, North Sydney, Australia, 2007.
- [3] BlueScope Lysaght, *The Lysaght Referee*, 34th Edition, BlueScope Steel Limited, 2019.
- [4] H. Adeli, A. Karim, Neural network model for optimization of cold-formed steel beams, *ASCE Journal of Structural Engineering* 123 (1997) 1535–1543.
- [5] R.L. McGavin, H. Bailleres, J. Fehrmann, B. Ozarska, Stiffness and density analysis of rotary veneer recovered from six species of Australian plantation hardwoods, *BioResources* 10 (2015) 6395–6416.
- [6] A. Karim, H. Adeli, Global optimum design of cold-formed steel hat-shape beams, *Thin-Walled Struct.* 35 (1999) 275–288.
- [7] J. Lee, S.-M. Kim, H.-S. Park, B.-H. Woo, Optimum design of cold-formed steel channel beams using micro Genetic Algorithm, *Eng. Struct.* 27 (2005) 17–24.
- [8] J. Ye, I. Hajirasouliha, J. Becque, A. Eslami, Optimum design of cold-formed steel beams using Particle Swarm Optimisation method, *J. Constr. Steel Res.* 122 (2016) 80–93.
- [9] B. Wang, G.L. Bosco, B.P. Gilbert, H. Guan, L.H. Teh, Unconstrained shape optimisation of singly-symmetric and open cold-formed steel beams and beam-columns, *Thin-Walled Struct.* 104 (2016) 54–61.
- [10] W. Lu, *Optimum Design of Cold-Formed Steel Purlins Using Genetic Algorithms*, PhD Thesis, Helsinki University of Technology, Helsinki, Finland, 2003.
- [11] J. Leng, Z. Li, J.K. Guest, B.W. Schafer, Shape optimization of cold-formed steel columns with fabrication and geometric end-use constraints, *Thin-Walled Struct.* 85 (2014) 271–290.
- [12] J.M.S. Franco, J.P. Duarte, E.d.M. Batista, A. Landesmann, Shape Grammar of steel cold-formed sections based on manufacturing rules, *Thin-Walled Struct.* 79 (2014) 218–232.
- [13] J. Ye, I. Hajirasouliha, J. Becque, K. Pilakoutas, Development of more efficient cold-formed steel channel sections in bending, *Thin-Walled Struct.* 101 (2016) 1–13.
- [14] S.M. Mojtabaei, J. Ye, I. Hajirasouliha, Development of optimum cold-formed steel beams for serviceability and ultimate limit states using Big Bang-Big Crunch optimisation, *Eng. Struct.* 195 (2019) 172–181.
- [15] J. Leng, J.K. Guest, B.W. Schafer, Shape optimization of cold-formed steel columns, *Thin-Walled Struct.* 49 (2011) 1492–1503.
- [16] M. Moharrami, A. Louhghalam, M. Tootkaboni, Optimal folding of cold formed steel cross sections under compression, *Thin-Walled Struct.* 76 (2014) 145–156.
- [17] J.F.A. Madeira, J. Dias, N. Silvestre, Multiobjective optimization of cold-formed steel columns, *Thin-Walled Struct.* 96 (2015) 29–38.
- [18] B.P. Gilbert, T.J.-M. Savoyat, L.H. Teh, Self-shape optimisation application: optimisation of cold-formed steel columns, *Thin-Walled Struct.* 60 (2012) 173–184.
- [19] B.P. Gilbert, L.H. Teh, H. Guan, Self-shape optimisation principles: optimisation of section capacity for thin-walled profiles, *Thin-Walled Struct.* 60 (2012) 194–204.
- [20] B. Wang, B.P. Gilbert, H. Guan, L.H. Teh, Shape optimisation of manufacturable and useable cold-formed steel singly-symmetric and open columns, *Thin-Walled Struct.* 109 (2016) 271–284.
- [21] B. Wang, B.P. Gilbert, A.M. Molinier, H. Guan, L.H. Teh, Shape optimisation of cold-formed steel columns with manufacturing constraints using the Hough transform, *Thin-Walled Struct.* 106 (2016) 75–92.
- [22] J. Holland, *Adaptation in Natural and Artificial Systems*, University of Michigan Press, Ann Arbor, 1975.
- [23] G.W. Flake, *The Computational Beauty of Nature*, 1998. Cambridge, England.
- [24] B.W. Schafer, Review: the Direct Strength Method of cold-formed steel member design, *J. Constr. Steel Res.* 64 (2008) 766–778.
- [25] AS/NZS 4600, *Cold-formed Steel Structures*, Standards Australia, Sydney, Australia, 2018.

- [26] S. Adany, B.W. Schafer, Buckling mode decomposition of single-branched open cross-section members via finite strip method: Derivation, *Thin-Walled Struct.* 44 (2006) 563–584.
- [27] S. Adany, B.W. Schafer, Buckling mode decomposition of single-branched open cross-section members via finite strip method: application and examples, *Thin-Walled Struct.* 44 (2006) 585–600.
- [28] Y.K. Cheung, *Finite Strip Method in Structural Analysis*, Pergamon Press, Inc., New York, N.Y., 1976.
- [29] B.W. Schafer, S. Adany, Buckling analysis of cold-formed steel members using CUFSM: conventional and constrained finite strip methods, in: R.A. LaBoule, W. W. Yu (Eds.), *Proceedings of the 18th International Specialty Conference on Cold-Formed Steel Structures*, U.S.A., Orlando, Florida, 2006, pp. 39–54.
- [30] H. Adeli, N.-T. Cheng, Augmented Lagrangian genetic algorithm for structural optimization, *J. Aero. Eng.* 7 (1994) 104–118.
- [31] C. Ren, L.-Y. Li, J. Yang, Bending analysis of partially restrained channel-section purlins subjected to up-lift loadings, *J. Constr. Steel Res.* 72 (2012) 254–260.
- [32] L.-Y. Li, C. Ren, J. Yang, Theoretical analysis of partially restrained zed-purlin beams subjected to up-lift loads, *J. Constr. Steel Res.* 70 (2012) 273–279.
- [33] T. Gao, C.D. Moen, Predicting rotational restraint provided to wall girts and roof purlins by through-fastened metal panels, *Thin-Walled Struct.* 61 (2012) 145–153.
- [34] C. Zhao, J. Yang, F. Wang, A.H.C. Chan, Rotational stiffness of cold-formed steel roof purlin–sheeting connections, *Eng. Struct.* 59 (2014) 284–297.
- [35] G.J. Hancock, *Design of Purlins*, 2018.
- [36] BlueScope Lysaght, *SPANDEK Design and Installation Guide*, BlueScope Steel Limited, 2018.
- [37] W. Lu, P. Makelainen, Augmented Lagrangian genetic algorithms for optimal design of hat-shaped cold-formed steel profile, in: *Proceedings of the 9th International Conference: Modern Building Materials, Structures and Techniques*, Vilnius, Lithuania, 2007.
- [38] N. Talebian, B.P. Gilbert, C.H. Pham, R. Charriere, H. Karampour, Parametric studies and design rules for local and distortional biaxial-bending capacity of cold-formed steel storage-rack uprights, *ASCE Journal of Structural Engineering* 146 (2020), 04020009.
- [39] J.-H. Zhang, B. Young, Finite element analysis and design of cold-formed steel built-up closed section columns with web stiffeners, *Thin-Walled Struct.* 131 (2018) 223–237.
- [40] M.R. Haidarali, D.A. Nethercot, Finite element modelling of cold-formed steel beams under local buckling or combined local/distortional buckling, *Thin-Walled Struct.* 49 (2011) 1554–1562.
- [41] B.W. Schafer, Z. Li, C.D. Moen, Computational modeling of cold-formed steel, *Thin-Walled Struct.* 48 (2010) 752–762.
- [42] Abaqus, *Abaqus Ver. 6.14 - User Manual*, (Dassault Systèmes), Vélizy-Villacoublay, France, 2014.
- [43] K.W. Karren, Corner properties of cold-formed shapes, *J. Struct. Div.* 93 (1967) 401–433.
- [44] K.F. Chung, K.H. Ip, Finite element modeling of bolted connections between cold-formed steel strips and hot rolled steel plates under static shear loading, *Eng. Struct.* 22 (2000) 1271–1284.